Study of porous SiOCH patterning using metallic hard mask: challenges and solutions

Nicolas Posseme, Thibaut David, Thierry Chevolleau, Maxime Darnon, Fanny Bailly, Régis Bouyssou, Julien Ducote, Hamed Chaabouni, Mohamed El Kodadi, Christophe Licitra, et al.

Study of porous SiOCH patterning using metallic hard mask: challenges and solutions

N.Posseme [a], T.David [a], T.Chevolleau [b], M.Darnon [b],
F.Bailly [c], R.Bouyssou [c], J.Ducote [c], H. Chaabouni [b], M. El Kodadi [b], C. Licitra [a]
C.Verove [c] and O.Joubert [b]

[a]CEA-LETI, Minatec campus, 38054 Grenoble, France
[b]LTM-CNRS/UJF/INP, 38054 Grenoble, France
[c]STMicroelectronics, 38926 Crolles cedex, France
Contact : nicolas.posseme@cea.fr

The choice of copper/low-k interconnect architectures is instrumental in achieving high device performances. Today, the implementation of porous low-k materials becomes mandatory in order to compensate metal resistance increase upon RC product. However, their introduction, which was initially planned for the 65nm technological node, was delayed to 45nm node due to integration issues. Using an integration strategy which combines porous SiOCH materials and metal hard masks, the difficulties and possible solutions are presented in this paper with emphasis on plasma etching.

I. Introduction

One of the most serious challenges in semiconductor manufacturing is to produce low cost integrated circuits as well as to develop high performance devices. On a technical point of view, a serious problem is that electric signal propagation through metal interconnects is delayed by the resistance (R) of the metal lines and the capacitance (C) between adjacent metal lines. Nowadays, the chosen way to decrease the runtime delays and thus the RC product is to use a less resistive metal (ie. copper) and decrease the power consumption and cross-talk (given by the capacitance) by integrating lower dielectric constant insulators [1]. To achieve this, many low-k materials have been investigated. There are two categories of materials: silicon containing (silica-based and silsesquioxane) or non silicon containing [2-5] materials presenting different advantages and drawbacks in term of chemical and physical properties, thermal stability and expansion, etc.. Finally, from the 90 nm technological node, the semiconductor industry selected $Si\text{-}CH_3$ containing organosilicate materials close to the well known SiO_2 [6]. These materials present k value of about 3 and can be reduced further by introducing porosity leading in the meantime to a weakening of its mechanical properties [2]. The introduction of porous SiOCH material was initially planned for the 65nm technological node, but the complexity of their introduction delayed their introduction for the 45nm interconnect technology node. For instance, previous study performed on blanket wafers, has shown that porous SiOCH materials are sensitive to fluorocarbon based plasma. These results obtained on spin-on p-SiOCH films presenting a porosity variation between 40% and 50% demonstrated the film degradation (methyl group depletion and moisture uptake) directly scales with porosity in the material [7].

In this paper, we propose to analyse the issues revealed during the integration of a porous low-k material (deposited by plasma enhanced chemical vapor deposition, with dielectric constant 2.35), and the associated solutions from an etching point of view. P-SiOCH line patterning can be achieved using different hard mask strategies (metallic or organic hard masks) [8-10], both presenting advantages and drawbacks in terms of etching performance etc. [11]. In this paper we will only focus on the metallic hard mask approach to discuss the etching challenges.

II. Experimental

The presentation of p-SiOCH integration difficulties with a metallic hard mask approach will be discussed and characterized using several techniques briefly described below.

II.1 Porous SiOCH materials

In this study, porous SiOCH material presenting a porosity of 28% with dielectric constant 2.35 is investigated. These materials are deposited by plasma enhanced chemical vapor deposition (PECVD) in a Producer^{TM} mainframe from Applied Materials. Using a co-injection gas feed, two precursors are simultaneously vaporized (Diethoxymethylsilane ($C_5H_{14}O_2Si$, DEMS) as a matrix precursor and a norbornadiene (NBD) component as a porogen precursor and injected in a capacitively coupled plasma chamber operated at 13.56 MHz. After depositing the hybrid film (SiOCH matrix plus the porogen), a thermal curing assisted by ultraviolet radiations is performed at 400 °C under He environment in a curing chamber to facilitate the porogen removal and generate the porous film [12, 13].

II.2 Porous SiOCH integration with a metallic hard mask

In this work, the patterning of porous SiOCH trenches is performed using a metallic hard mask with the following stack on silicon substrate: porous carbon-doped silicon-oxide (PECVD p-SiOCH, with 28% porosity) / PECVD silicon dioxide (SiO_2) / titanium nitride deposited by physical vapor deposition (PVD TiN) and BARC/193 nm resist patterns.

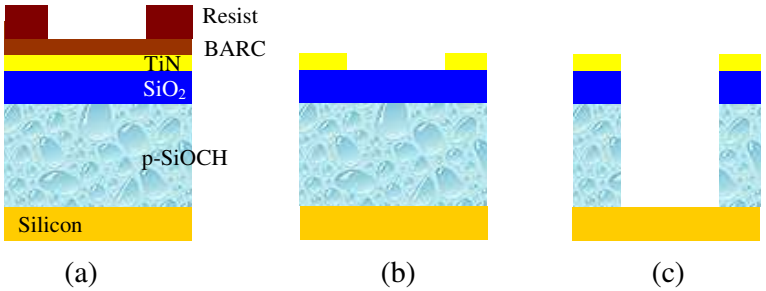

Fig. 1: Metallic hard mask (MHM) description: (a) Line lithography with organic BARC, (b) HM etching and resist stripping, (c) Line etching.

In the metallic hard mask (MHM) approach, a thin metallic hard mask layer is deposited on the top of a dense dielectric layer (SiO_2) which encapsulates the underlying p-SiOCH material. The trench photolithography is performed using a positive tone photoresist coupled with a bottom antireflective layer (BARC) (Fig.1(a)).

The BARC and titanium nitride layers are etched in a chlorine-based chemistry (Cl_2/BCl_3) using an inductively coupled plasma (ICP), followed by resist stripping in an O_2 micowave plasma (Fig.1(b)). Then the SiO_2 capping and porous SiOCH layers are patterned in fluorocarbon (FC) based plasmas ($C_4F_8/N_2/Ar/O_2$) using a multi-frequency capacitive coupled plasma (CCP) etcher (Fig.1(c)).

II.3 Characterization techniques of p-SiOCH modification

In this study, the film modification will be presented through experiments performed on blanket wafers (to represent bottom p-SiOCH film modification) and on patterned wafers to analyse the sidewall film modifications. Different complementary techniques like X-ray photoelectron spectroscopy (XPS), infrared spectroscopy, decoration method and ellipsometric porosimetry (EP) will be used.

II.3.1 X-ray Photoelectrons spectroscopy (XPS)

The surface composition of the p-SiOCH after FC based plasma exposure has been analyzed on 300mm blanket and patterned wafers using ex-situ XPS analyses.

XPS analyses spectra are performed on blanket and patterned wafers using a Thermo Fisher Scientific Theta 300 spectrometer operating with a monochromatic Al Kα x-ray source ($h\upsilon$ = 1486.6 eV) and an electron energy analyzer operating in a constant pass energy mode of 20eV. Chemical compositions are derived from the areas of the different XPS spectra. Spectral decomposition is performed to extract the Si2p, O1s, C1s, N1s and F1s peak intensities. Individual line shapes are simulated with the combination of Lorentzian and Gaussian functions. The background subtraction is performed by using a Shirley function. After XPS analysis, the integrated intensities are divided by the theoretical Scofield (S) cross section (C1s:1; O1s:2.93; Si2p:0.82; F1s:4.43; N1s:1.8). The sum of the concentration of the different elements present on the analysed surface is equal to 100%. The hydrogen content is not taken into account in this calculation since hydrogen cannot be detected by XPS. More details of the experimental characterization conditions can be found elsewhere [7, 14].

The determination of the p-SiOCH sidewalls film composition is achieved thanks to the specific die where different zones exhibiting regular arrays of lines, blanket substrate and unpatterned mask material are present. From the concentrations of the different elements present on a blanket area (covered with the metal hard mask) and by recording XPS spectra in the perpendicular mode in dense features, we can obtain the chemical composition of the patterns sidewalls. However, the contributions originating from the SiO_2 sidewalls and those originating from the p-SiOCH sidewalls cannot be separated. The experimental protocol is described in more details elsewhere [15]. To overcome this issue we developed an improvement of the experimental procedure by using the subtraction between two analysed patterned areas (Fig.2).

Two XPS acquisitions are performed in the perpendicular mode with contributions originating from the top (TiN), SiO_2 and p-SiOCH sidewalls of the features in a large pitch (LP) (Fig.2(a)) is performed first. A second XPS acquisition is then performed in a smaller pitch (SP) where contributions originate from the top (TiN) and SiO_2 sidewalls of the features only (Fig.2(b)).

Assuming the compositions on top of metallic hard mask and sidewall of SiO_2 trenches are similar between LP and SP, the substraction of the signal (LP-SP) corrected to the ration P2/P1 provides the contribution of the p-SiOCH sidewalls only. For these specific measurements the TiN and SiO_2 thickness are 15 nm and 125 nm, respectively while the p-SiOCH thickness is set at 670 nm.

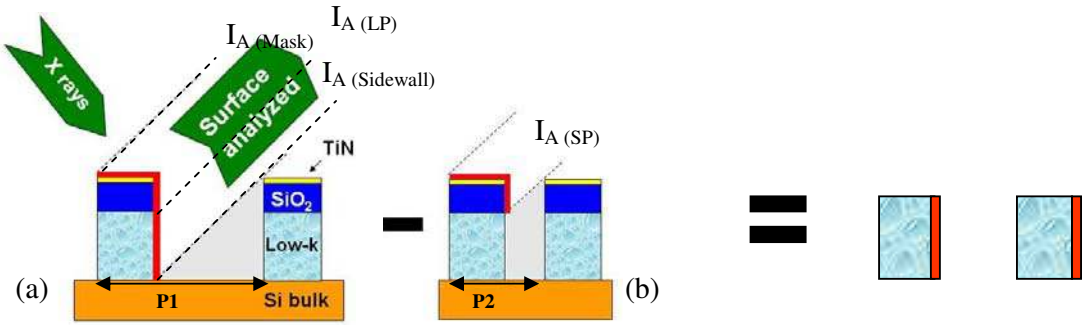

Fig. 2: Desciption of XPS analyses on patterned wafers in large pitch (P1 = 800nm, feature dimension= 200nm) (a) and small pitch (P2= 340nm, feature dimension = 200nm) (b) areas to obtain p-SiOCH sidewall film composition.

Using this experimental protocol we can determine the p-SiOCH sidewall composition as follows:

- The concentrations of Ti, O, N, F, Si, and C atoms are extracted from the Ti2p, O1s, N1s, F1s, Si2p and C1s core-level energy regions, respectively.
- The background subtraction is performed using a Shirley function calculated from a numerical iterative method.
- The intensity of photoelectrons coming from hard mask and SiO_2 ($I_{A(Mask)}$) in large area is calculated as following:

$$I_A(Mask) = I_A(SP) * \frac{P2}{P1}$$

- The sidewall porous SiOCH intensity is calculated for each element (extracted from the Ti2p, O1s, N1s, F1s, Si2p and C1s core-level energy regions).

For a given element A :

$$I_A(Sidewall) = I_A(LP) - I_A(Mask)$$

$$I_A(Sidewall) = I_A(LP) - I_A(SP) * \frac{P_2}{P_1}$$

- Then the concentration of the given element A is quantified with respect to the other elements detected as follows :

$$[A] = \frac{\frac{I_A}{S_A}}{\sum_k \frac{I_k}{S_k}}$$

This method gives a rough estimate of the p-SiOCH composition on the feature sidewalls.

II.3.2 Infrared Spectroscopy

Infrared Spectroscopy analyses in transmission (T-FTIR) and in multi internal reflection (MIR-FTIR) are performed using a Bruker IFS-55 FTIR spectrometer. For the T-FTIR analyses, the IR beam passes trough the wafer and is focused on a DTGS detector. The T-FTIR mode covers a spectral range from 400 to 4000 cm^{-1}. For the MIR-FTIR analyses, the sample is coupled to the s-polarised IR beam with two silicon prisms whose spacing is adjusted to Z=6 cm. A s-polarized IR beam coming from FTIR spectrometer is directed on the coupling area of the input prism, which ensures optical tunneling inside the wafer. After being internally reflected about 100 times in our conditions (with an incidence angle of 34° and a wafer thickness of about 600 µm), the IR beam is coupled out of the wafer by the second prism and focused onto a liquid-N_2-cooled HgCdTe detector [16, 17]. The MIR technique is 100 times more sensitive than the standard transmission mode (T-FTIR). The IR beam propagates inside the wafer so that the samples have to be double-side polished. The MIR-FTIR mode covers a spectral range from 2600 to 4000 cm^{-1}. The spectral range is lower than this with the T-FTIR mode due to absorption of the IR beam at higher wave numbers into the silicon wafer during the internal reflection. Spectra are recorded with a 2 cm^{-1} spectral resolution and an average of 32 scans and 200 scans with the T-FTIR and MIR-FTIR modes, respectively. Before the spectrum acquisition, 5 min nitrogen purge is performed in the spectrometer to remove H_2O and CO_2 vapor. The baseline of IR spectra is removed with the software "Resolution Pro" using a spline curve. For T-FTIR acquisition, a reference spectrum is measured using a virgin silicon wafer in order to remove the spectral contribution of the silicon wafer and the optical bench.

II.3.3 Spectroscopic Ellipsometry (SE)

The refractive index, extinction coefficient and the thickness of the porous SiOCH films were measured using a UV-visible spectroscopic ellipsometry from Jobin Yvon. To determine those values, the ellipsometry parameters were fitted with an absorbent Cauchy model for the porous SiOCH.

II.3.4 HF decoration method

We can determine the thickness of the modified p-SiOCH film thanks to spectroscopic ellipsometry (SE) using the decoration technique. This technique relies on the principle that the pristine porous SiOCH film is not consumed during hydrofluoric acid (HF) dip while the modified layer (with moisture uptake and carbon depletion) is removed [18-20]. The thickness of the remaining p-SiOCH film is determined by spectroscopic ellipsometry (SE) before and after HF dip allowing the thickness of the modified layer to be determined. On patterned wafers, the wafers are cleaved and dipped into a 1% diluted HF solution during 15 s after p-SiOCH etching. Using this protocol, we can estimate the thickness of the damaged layer on the trench sidewalls by using scanning electron microscopy (SEM). Before SEM observations, the trenches are filled with resist in order to prevent potential feature collapse during SEM exposure.

II.3.4 Ellipsometric porosimetry (EP)

The Ellipsometric porosimetry technique has been used to characterize the impact of FC based plasma exposure on the mean pore radius, the pore size distribution and the open porosity of p-SiOCH. Ellipsometry porosimetric measurements are performed in the

visible range on an EP12 ellipsometric porosimeter from SOPRALAB [21]. It consists of a rotating polarizer spectroscopic ellipsometer coupled with a vacuum chamber which is operated in a pressure range between 10^{-3} Torr and the saturation vapor pressure (Ps) of the adsorptive. For a solvent partial pressure P/P_S, the adsorptive penetrates into the low-k and condenses into the pores leading to an increase of the refractive index. Indeed the vapour of the adsorptive condenses in the pores for a vapor pressure (P_a) lower than a flat surface liquid (P_s) and the value of partial pressure P_a/P_s depends on the pore size, surface tension and molar volume of the solvent.

Two solvents are used as adsorptive: methanol (P_s~105 Torrs, n_{Met}=1.329 at 633 nm) and water (P_s~20 Torrs, n_{Water}=1.33 at 633 nm). The methanol solvent penetration kinetics over time through the damaged p-SiOCH surface gives information on the sealing of the surface [22]. The degree of hydrophilization associated to the plasma damage is determined with water vapors thanks to a dedicated bi-layer analysis. The spectra are saved with a CCD detector between 1.5 and 4 eV at an angle of incidence set at 60.25°. Thickness and refractive index of the layers are calculated from the ellipsometric data as a function of the relative pressure ($P_{rel}=P/P_s$, with P the chamber pressure) using a Cauchy law in adjunction with a Lorentz oscillator to take into account the absorption band in the ultraviolet region. On the basis of the Lorentz-Lorenz effective medium approximation, the volume fraction of solvent adsorbed in the pores is calculated as described in a previous paper [21].

The p-SiOCH sidewall modification of patterned structures differs from at the bottom of the trenches. An innovative non-destructive method has recently been developed to measure the porous properties of p-SiOCH patterned layers as integrated into circuit called Scatterometric Porosimetry (SP) [23, 24]. It mainly consists in the use of an EP tool (previously described) to record the scatterometric response of periodic structures made of porous material as a function of the relative pressure of the solvent. The patterned structures are chosen to have a critical dimension which is equivalent to the interconnect line size except that they typically consist of parallel periodic lines. The porous properties are subsequently extracted from the SP measurement with the use of a specially-developed scatterometric modeling [23]. For such analyses, patterning of the porous SiOCH trenches is performed using a metallic hard mask (Figure 1) with the following film thickness: a titanium nitride layer (15 nm thick), an oxide capping layer (125 nm thick) and the porous dielectric material (670 nm thick and 28% of porosity).

II.3.5 Capacitance measurement: Mercury Probe

The dielectric constant of blanket films has been calculated before and after the different plasma exposures using capacitance-voltage (C-V) measurements at 0.1 MHz. C-V measurements have been performed using a mercury probe capacitance measurement (C-V) system (model SSM495).

II.5.1 Bottom line roughness

Atomic force microscopy (AFM) measurements are performed at ambient atmosphere with a Nanoscope III multimode microscope from Digital Instruments. The RMS roughness is determined by tapping mode AFM with the measurement of the standard deviation of the height distribution (RMS). More detail of the measurement can be found elsewhere [25].

III. P-SiOCH film modification induced by fluorocarbon based plasma

A low-k material must withstand different integration steps, in particular the etching step. However, p-SiOCH materials are much more sensitive than SiO_2 to plasma exposure (chemical and physical impact of the plasma may induce p-SiOCH damage which in turn alters the dielectric film properties) [2]. A large contribution of the sensitivity comes from porosity introduction [7]. In this section, we propose to evaluate the sensitivity of p-SiOCH (PECVD p-SiOCH with 28% porosity) material after trench etching under FC based plasmas exposure. The bottom (estimated thanks to experiment performed on blanket wafers) and sidewalls p-SiOCH film modifications are compared and the potential solutions are discussed.

III.1 Bottom p-SiOCH film modification after partial etching

In this part, experiments have been performed on blanket p-SiOCH films to estimate bottom p-SiOCH film modifications induced by fluorocarbon plasmas. First, the surface and structural composition of the pristine p-SiOCH are investigated. Then to mimic material consumption for 45 nm technology node, 120 nm of p-SiOCH has been etched in CF_4 /C_4F_8/ N_2/Ar used for p-SiOCH trench etching. P-SiOCH film has been analyzed on blanket wafers by XPS, T-FTIR and MIR-FTIR before and after partial etching.

III.1.1 Surface analyses

The XPS survey spectrum of as-deposited p-SiOCH (not shown), indicates the presence of silicon, oxygen and carbon (hydrogen is not detected by XPS). The surface composition, reported in Table 2, shows that p-SiOCH is composed of Si (36%), O (40%) and C (24%).

Table 2: XPS surface composition of p-SiOCH (porosity of 28% and k=2.35) on blanket and patterned wafers after FC etching

Material	Si(%)	O(%)	C(%)	F(%)	N(%)	Ti (%)
p-SiOCH as deposited (blanket wafer)	36	40	24	0	0	0
p-SiOCH after FC etching (blanket wafer)	25	30	34	8	3	-
p-SiOCH after FC etching (sidewall)	17	19	38	23	1	2

After p-SiOCH partial etching in CF_4 /C_4F_8/ N_2/Ar plasma, XPS analyses reveal that the surface is composed of 25%Si, 30%O, 34% C, 8%F and 3%N (See Table 2).

III.1.2 Volume analyses

T-FTIR analyses

Fig.3 shows a typical T-FTIR spectrum of the as deposited porous SiOCH. In the 1000 to 1500 cm^{-1} spectral range, T-FTIR spectrum exhibits three main absorption bands at 1022, 1065 and 1140 cm^{-1} corresponding to C-Si-O and Si-O-Si stretching vibration bands [21, 26]. Two additional peaks are also observed at 1275 cm^{-1} and 2960 cm^{-1}, which are assigned to the $Si-CH_3$ and $C-H_3$ vibration bands, respectively. After p-SiOCH exposure to FC based plasma, the FTIR spectrum (see Fig.3) exhibits the same vibration modes as those detected in the pristine material.

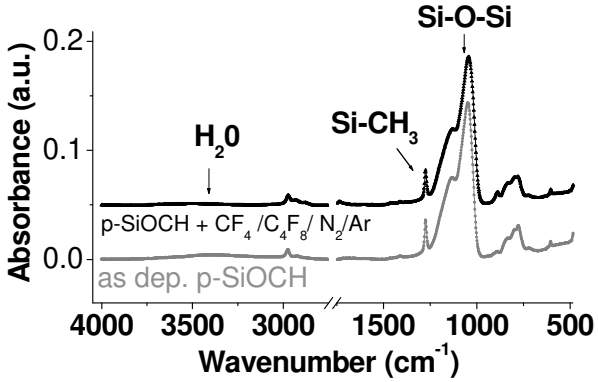

Fig. 3: T-FTIR spectra of p-SiOCH before and after partial etching in FC based plasma

Based on these spectra, the methyl content in the film can be monitored by calculating the peak area ratio from the T-FTIR spectra:

$$R_{SiCH3} = \frac{A_{Si-CH_3}}{A_{Si-CH_3} + A_{Si-O-si}}$$

where $R_{Si\text{-}CH3}$ represents the methyl ratio, $A_{Si\text{-}CH3}$ the area of the Si-CH_3 vibration bands and $A_{Si\text{-}O\text{-}Si}$ the area of the Si-O-Si vibration bands[14, 34]. In these conditions, after partial etching, the methyl depletion is estimated at about 25% compared to the pristine material.

MIR-FTIR analyses

In the 2700 to 4000 cm^{-1}spectral range, the MIR-FTIR spectrum of porous SiOCH after partial etching shows vibration bands which are assigned to OH and CH_x bonds (see Fig.4) [16].

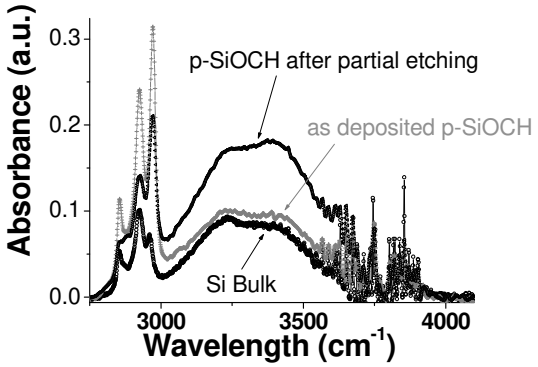

Fig. 4: MIR-FTIR spectra of p-SiOCH before and after partial etching in FC based plasma

CH_x vibration bands are assigned to four peaks: CH_2 at 2860 and 2930 cm^{-1}, CH_3 at 2880 and 2965 cm^{-1}. The large OH vibration band into the modified porous SiOCH can be assigned to four peaks: two from Si-OH (isolated and linked) and two from water H_2O (free and bonded) at 3672, 3551, 3425 and 3225 cm^{-1}, respectively [17, 20, 27]. This broad OH vibration bands exhibits the same intensity as the OH vibration band originating from the Si bulk spectrum. Therefore the OH vibration is mainly attributed to the Si bulk coming from the native silicon oxide and it is then difficult to prove the presence of OH bonds in the as deposited materials. It has to be noticed that the OH vibration bands are hardly detected on the T-FTIR spectra due to the lower sensitivity compared to MIR-FTIR technique.

After partial etching, the absorption of the OH vibration bands is much higher than in the as deposited porous SiOCH. This result shows an increase in Si-OH bonds formation due to water uptake with free and bonded H_2O. It has to be noticed that no OH vibration bands have been observed with FTIR measurement due to the lack of sensitivity. After partial etching, the CH_x peaks (CH_3 and CH_2) are slightly lower than those of the as deposited porous SiOCH indicating lower methyl depletion in the remaining porous SiOCH (which is in good agreement with the FTIR analyses).

III.1.3 Depth modification of the p-SiOCH film

Using decoration method

We have then determined the thickness of this modified p-SiOCH film thanks to spectroscopic ellipsometry (SE) using the decoration technique previously described. Based on this protocol, after the etching process, the damaged layer is estimated to be about 30 nm thick. We can notice that after the HF dip which removes the modified layer, no methyl depletion is evidenced after partial etching (not shown) indicating that the methyl depletion is mainly localized in the modified layer.

Using EP

The hydrophilic properties of the modified layer have been also determined with EP measurement using water as solvent. Based on the protocol previously described, the thickness of the modified layers is estimated after FC based plasma exposure to be 29nm.

Both techniques show similar modified layer thickness confirming the correct estimation of modified layer thickness on blanket wafers.

III.1.4 Impact of the modified layer on pore sealing

The impact of the thick hydrophilic modified layer on open porosity and permeability has been investigated thanks to EP analyses with methanol as solvents (Fig.5). The degree of porosity is followed as function of time at a fixed pressure (0.8 of vapour pressure) to determine the total porosity and permeability of the porous SiOCH modified layer (as described in the previous section). The open porosity which is measured at the plateau remains the same as the pristine material (of about 27%) with or without partial etching. This result demonstrates no significant change in pore density and pore size in the remaining porous SiOCH films. This also indicates that the porosity of the modified layer is similar to the pristine material.

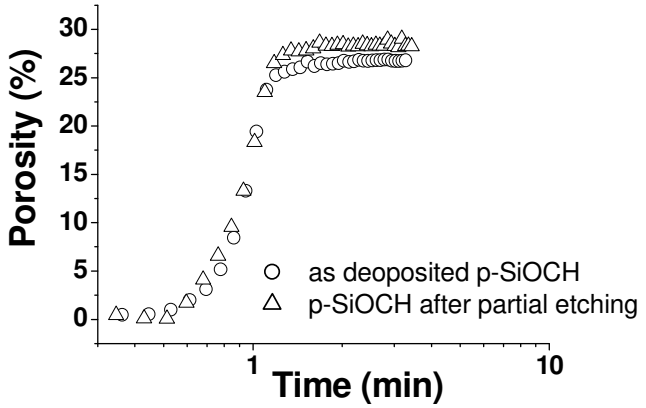

Fig. 5 : Evolution of porosity as a function of time at a fixed relative pressure (0.8Ps) with methanol thanks to EP measurement

These experiments performed on blanket p-SiOCH show that the film is altered under FC based plasma exposure leading to the formation of a hydrophilic perturbed layer depleted in methyl groups. This perturbed layer induces an increase of the dielectric constant from 2.35 to 2.7 after partial etching. These results are similar than those observed for a spin-on p-SiOCH material [7]. In this previous study, we demonstrated that the film modification could be assigned to fluorine reactive species diffusion and to the impact of the ion bombardment. In the first case, the diffusion of fluorine atoms into the porous material generates an important degradation of the material since fluorine is very reactive toward carbon and silicon. While in the second case, the ion bombardment can break Si–O, Si–CH_3, and C–H bonds [7].

The study of the film modification performed on blanket wafer gives a good picture of the p-SiOCH film modification at the bottom of trenches. However, can we draw similar conclusion on the p-SiOCH sidewalls modification? These results are now compared with the film modification analyses performed on patterned structure.

III.2 p-SiOCH film sidewall modification after partial etching

After patterning of p-SiOCH trenches in CF_4 /C_4F_8/ N_2/Ar plasma, no sidewall modification is clearly evidenced using the decoration technique. This can be attributed to of a lack of sensitivity of this technique for thin damage layer (Fig.6).

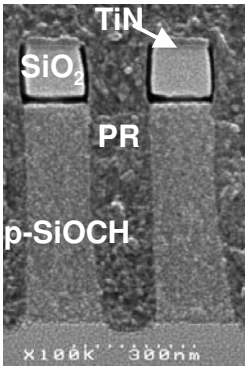

Fig. 6: Estimation of the sidewall modification of p-SiOCH trenches after CF_4 /C_4F_8/ N_2/Ar etching using the decoration technique

Indeed the hydrophilic properties of the modified layer determined with SP measurement using water as solvent for EP analyses show different behaviour. The thickness of the damaged layer after etching is estimated in this case to 10 nm. This result tends to indicate the SP can be a more accurate technique to estimate the sidewall p-SiOCH film modification compared to decoration method.

Sidewall composition analyses performed using chemical topography analyses by XPS is summarized in Table 2. After etching, the presence of fluorocarbon species are detected on the p-SiOCH trench sidewalls while Ti is hardly detected. The presence of this small amount of Ti can be attributed either to the sputtering of the hard mask during etching or to the element concentration measurement error induced by the experimental protocol.

The impact of this FC layer formation on pore sealing was determined thanks to EP analyses using methanol as solvent. The methanol diffuses through the p-SiOCH sidewalls (not shown) indicating that p-SiOCH sidewalls are not pore sealed by the presence of the fluorocarbon layer. These results indicate that a CF_x layer grows on the p-SiOCH sidewalls (porosity of 28% and k = 2.35) during FC based plasma and that no pore sealing is induced by this CFx layer.

These observations are similar to previous observations on blanket wafers. Therefore, we can propose similar mechanisms to explain the p-SiOCH sidewall film modification which can be assigned to fluorine reactive species diffusion on the sidewalls leading to the creation of a hydrophilic layer. The effect of the ion bombardment being lowered since the ions deflected on the hard mask have lower energy than ions directly striking the p-SiOCH blanket wafers.

The whole results show that p-SiOCH (bottom and sidewall) is very sensitive to FC based plasma leading to the formation of a hydrophilic layer. This modified layer cannot be neglected since it alters the dielectric film properties. Indeed, k value measurement performed on blanket and patterned wafers shows that the perturbed layer leads to an increase of the dielectric constant. The k degradation is more pronounced as the thickness of porous SiOCH decreased [28]. Furthermore, the modified layer can also degrade the reliability performance of the dielectric layer. Therefore solution must be found to limit this p-SiOCH film modification or to improve the hydrophobic properties of the dielectric film after etching.

III.3 Solutions to limit p-SiOCH film modification

As suggested, p-SiOCH film modification (bottom and sidewalls) can be induced by fluorine, ion bombardment. Based on these results, different solutions were proposed in the literature to limit the p-SiOCH film modification.

One approach is to reduce fluorine reactive species diffusion in the film and the ion bombardment impact. This can be achieved by using high polymerising chemistries [7, 29]. Fig.7 shows that higher CH_2F_2 concentration in the CF_4/Ar gas mixture enables a reduction of the p-SiOCH (spin-on with 45% porosity) sidewall film modification. We have shown that such polymerizing etch chemistries lead to the formation of thick fluorocarbon layers on the p-SiOCH sidewalls which act as protective layers against fluorine diffusion inside the porous SiOCH material. Less sidewall modification are

observed in high polymerizing chemistries such as $CF_4/Ar/CH_2F_2$ which produce thicker FC layers on the sidewalls than in low polymerizing chemistries such as CF_4/Ar [29].

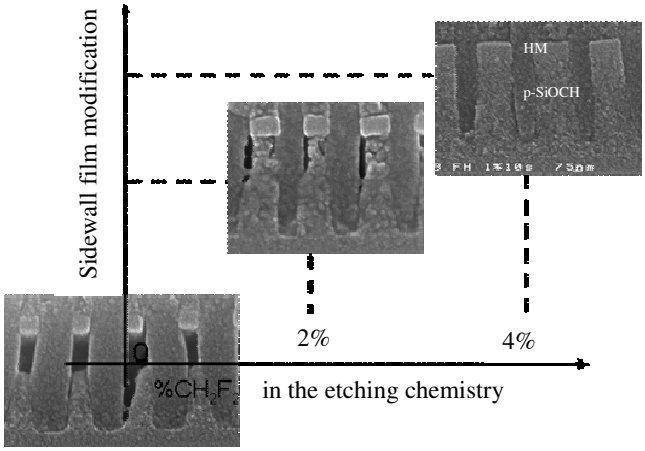

Fig. 7: Sidewall film modification of porous SiOCH (containing 45% porosity) after etching as a function of the CH_2F_2 concentration in CF_4/Ar gas mixture. The sidewall modification is determined using the decoration method.

Finally an emerging solution, as proposed in the literature, is to restore the hydrophobic properties of the modified layer by using a curing process: a silylation based process [28]. For instance, for the 45nm interconnect technology node, *Chaabouni et al* [28] show that after p-SiOCH (porosity of 25% and k=2.5) integration using a metallic hard mask approach, the integrated k value is about 3 (see Fig.8). After a post etching, restoration process using hexamethyldisilazane (HMDS: $(CH_3)_3$–Si–NH–Si–$(CH_3)_3$) enables to decrease the integrated k value to 2.6 close to the dielectric constant of the as-deposited p-SiOCH [28]. HMDS molecules selectively react with the silanol species and convert them into hydrophobic trimethyl-siloxy (–O–Si–$(CH_3)_3$) groups leading to an increase of the carbon content that prevents water uptake.

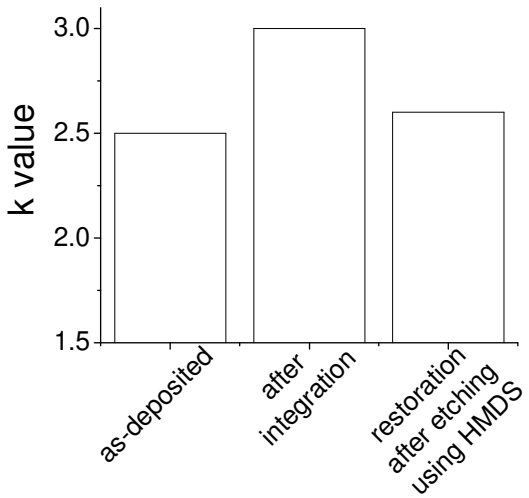

Fig. 8: Effect of sylilation process after etching on integrated k value [40]

III.4 Summary

Based on these results, we have shown that the damages of porous SiOCH sidewalls induced by FC plasma exposure are inevitable. They can alter dielectric film properties and generate an increase of dielectric constant and/or reliability degradation. The film modification due to reactive fluorine species diffusion and ion bombardment impact can be limited by using high polymerizing FC chemistries. In addition, a complementary solution is the restoration of the hydrophobic properties of the modified layer using silylation process.

We have shown the porosity introduction into SiOCH material induces higher film sensitivity to FC based plasma. But porosity introduction also leads to new issue like roughening of bottom line. In this case, are the solutions proposed to limit p-SiOCH damage compatible with the reduction of bottom line roughness?

IV. Bottom line roughness

As illustrated in Fig.9, increasing porosity of PECVD SiOCH material also leads to an increase of the bottom line roughness after line etching using a metal hard mask.

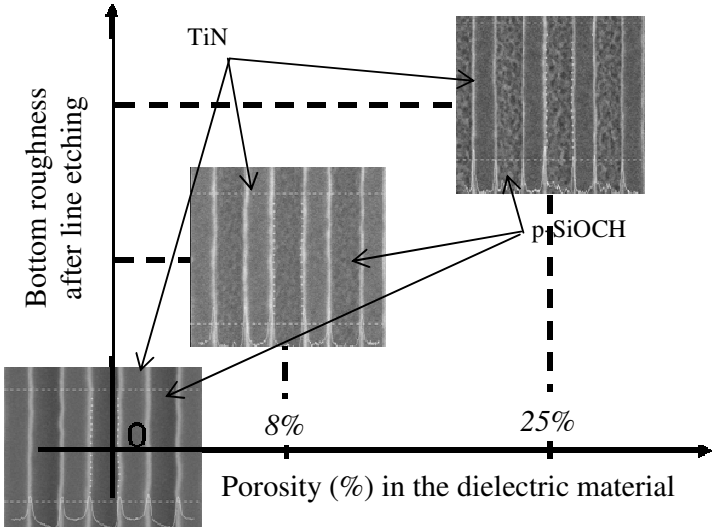

Fig. 9: Bottom line roughness evolution after line etching using a metal hard mask (with similar etching conditions) as a function of the p-SiOCH film porosity.

The impact of such a roughness on reliability performances has been evaluated by comparing two etching processes inducing either a low (Fig.10(a)) or a high bottom line roughness (Fig.10(b)). Whatever the etching chemistries, Fig.10(c) shows that the electromigration trend is not impacted while in the meantime, the time dependent dielectric breakdown (TDDB) lifetime is degraded (Fig.10(d)) when the bottom line roughness increase.

These results demonstrate that bottom line roughness strongly impact the TDDB. Therefore it's mandatory to limit the bottom line roughness in order to prevent TDDB degradation.

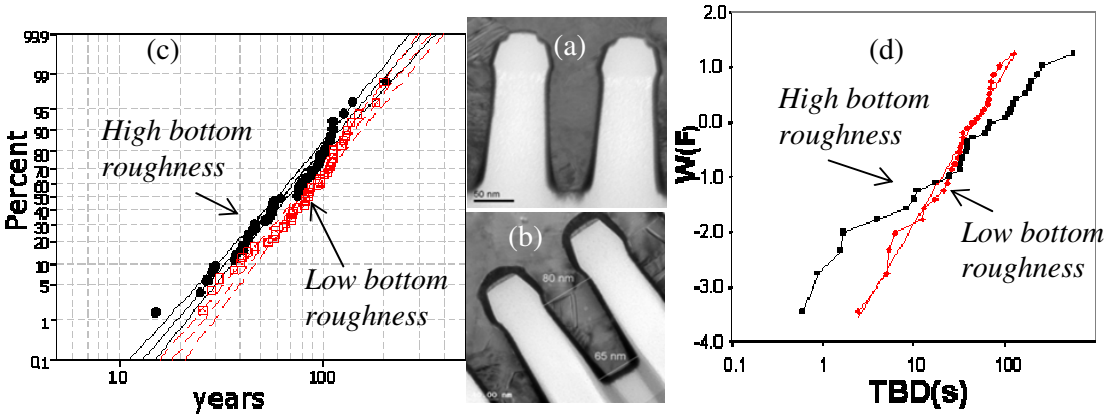

Fig. 10: Impact of the bottom line roughness high (a) and low (b) on electromigration (EMG) (c) and Time Dependent Dielectric Breakdown (TDDB) (d)

IV.1 Mechanism of bottom line roughness formation

The evolution of the roughness during plasma etch processes has already been studied [30 – 39]. Plasma processes usually smooth the etched surfaces. The isotropic component of the etch process, [33, 34] as well as the shadowing effect [40, 41] and the preferential sputtering of the material for off-normal ions [33, 42, 43] contribute to this effect during plasma etch processes. Nevertheless, several groups have reported that etched surfaces can also be roughened when exposed to plasma etch processes. [39, 44–47]. Several explanations such as preferential etching by re-emitted species [42, 43] or ion induced defects [46] have been proposed. However, recent studies [39, 47] tend to prove that etch induced roughness rather originates from micromasking phenomena induced by particles sputtered form the chamber walls during the etch process. Etch induced roughness has also been observed with p-SiOCH materials [30-33, 48]. These papers claim that, the fluorocarbon species deposited on the porous low-k surface induce p-SiOCH roughness. Tatsumi and Urata [49] suggest that low-k materials are roughened when a thin fluorocarbon layer (4 nm) is deposited on the material surface, while no fluorocarbon or thicker fluorocarbon layers do not lead to roughening. Yin *et al.* [31, 48] attribute the etching induced roughness to fluorocarbon species micromasking the material surface. They attribute the non uniform coverage of the surface to the presence of pores in the material. Lazzeri *et al.* [30] propose that the larger surface of porous materials leads to an incomplete coverage of the surface of the dielectric by the fluorocarbon layer, compared to dense dielectric layers. Due to this incomplete coverage, plasma species can directly interact with the low-k material, leading to harsher etch conditions and roughness. In both cases, the models assume that the roughness is created by an incomplete or non homogeneous coverage of the porous SiOCH surface by fluorocarbon species.

However in our experimental conditions close to the industrial ones, we demonstrated the roughness of porous SiOCH also occurs under fluorocarbon free plasma exposure (SF_6 plasma) suggesting complementary mechanism [25]. We proposed that: (1) during the first few seconds of the etch process, the surface of porous SiOCH materials gets denser. (2) Cracks are formed, leading to the formation of deep and narrow pits. (3) Plasma radicals diffuse through those pits and the pore network and modify the porous material at the bottom of the pits. (4) The difference in material density and composition between the surface and the bottom of the pits leads to a difference in etch rate and an amplification of the roughness [25].

IV.2 Solutions

Previous studies performed on blanket wafers indicate that the solution to smooth p-SiOCH during etching is to use highly polymerising FC chemistries [25]. The impact of the etch chemistry on porous SiOCH (p-SiOCH with 25% porosity) roughening is illustrated in Fig.11 by comparing the RMS roughness on blanket wafers induced by two different fluorocarbon based etching chemistries (different degrees of polymerizing). CH_2F_2 addition to CF_4/Ar (more polymerizing chemistry) induces a decrease in roughness.

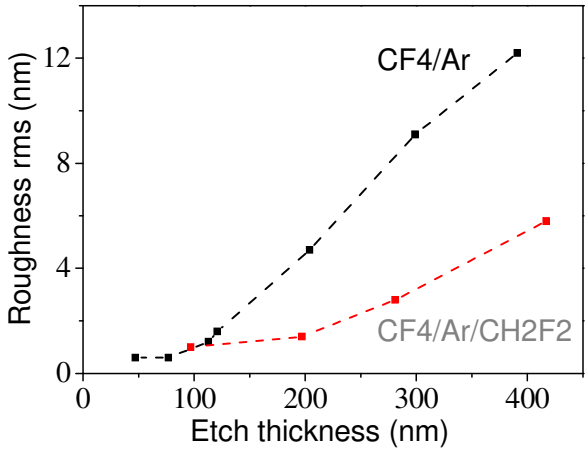

Fig. 11: Roughness evolution as a function of the etched depth for PECVD porous SiCOH (25% porosity) exposed to either CF_4 / Ar or CF_4 /Ar/CH_2F_2 plasmas. RMS value of the roughness measured by AFM.

However, this solution does not take into account the impact of the metallic hard mask on the p-SiOCH roughness formation. Indeed, on patterned wafers, in addition to the roughening of the p-SiOCH induced by fluorocarbon plasmas, additional roughness also originates from the micromasking induced by TiFx compounds coming from the TiN mask sputtering [50, 51]. The two key parameters to limit this metallic hard mask impact on roughness formation are the substrate temperature and the polymerising rate of the chemistry as illustrated below.

IV.2.1 Impact of Substrate temperature on p-SiOCH roughness formation

The impact of the substrate temperature on porous SiOCH roughness is illustrated Fig.12 by comparing the etching of p-SiOCH patterned structure using CF_4 based chemistry with two different substrate temperatures (higher or lower than 50°C). Increasing substrate temperature induces a lower bottom p-SiOCH roughness and straight profiles as evidenced by the SEM cross section in Fig.12(b). This trend is correlated with a lower titanium (5%) concentration at the bottom of trenches (determined by XPS), compared to lower substrate temperature where 12% titanium is measured by XPS (Fig.12(a)).
Therefore increasing substrate temperature above 50°C favours the formation of more volatile TiFx etch products and therefore decrease the micromasking induced effect of Ti based compounds deposited on p-SiOCH surfaces.

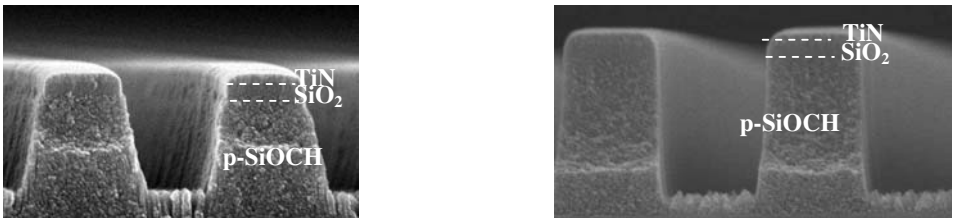

Fig. 12: Illustration of p-SiOCH etching in a metallic hard mask environment with a CF_4 based etching chemistry and a substrate temperature lower (a) or higher (b) than 50°C, respectively.

Another way to limit this metallic hard mask sputtering impact on p-SiOCH roughness formation is to protect it during etching. This can be achieved by using polymerizing chemistry.

IV.2.2 Impact of the etching chemistry on the p-SiOCH roughness

For substrate temperatures above 50°C, the impact of the etch chemistry on the porous SiOCH (p-SiOCH with 25% porosity) roughening is now presented in Fig.13 by comparing two CF_4 based etching chemistries with and without C_4F_8 addition.
With C_4F_8 addition to CF_4, a lower bottom p-SiOCH roughness is clearly observed on top SEM-CD pictures (Fig.13(b)) compared to CF_4 only (Fig.13(a)). XPS analyses reveal that C_4F_8 addition to CF_4 leads to the formation of a thick fluorocarbon layer on top of the metal hard mask (25% C and 13% F) decreasing its sputtering rate (5% titanium is detected at the bottom of trenches). Without polymerizing gas addition, the presence of higher titanium species concentration (10%) at the bottom of trenches correlated with a thinner fluorocarbon layer is detected on top of the metal hard mask (15% C and 10% F).

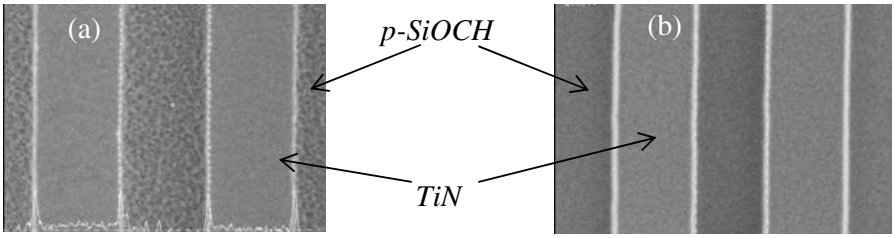

Fig. 13: Illustration of p-SiOCH etching in a metallic hard mask environment with either a CF_4 (a) or C_4F_8 (b) based etching chemistry for a substrate temperature higher than 50°C.

These results show that the use of highly polymerizing chemistries protect the metal hard mask, and limit its sputtering rate. Consequently, Ti based micromasking is reduced limiting the development of rough p-SiOCH surfaces.

IV.2.3 Summary

In summary, we have shown that the bottom surface roughness is directly related to the degree of SiOCH porosity and such a rouhgness can lead to the degradation of the TDDB while the electromigration is not altered.
The roughness formation is explained by different mechanisms such as the intrinsic p-SiOCH roughness developed under plasma exposure or micromasking coming from reactor wall conditioning, FC species or hard mask environment.

With a metal hard mask approach, the solution to limit p-SiOCH formation is to develop etching processes at substrate temperature above 50°C (to limit sputtered metal species condensation leading to micromasking) and the use of highly polymerising chemistry (to protect MHM with FC layer and also playing the role of p-SiOCH smoothing).

Conclusions

The major difficulties of p-SiOCH material integration using a metallic hard mask integration have been presented from the etching point of view. The first problem encountered with porosity introduction into SiOCH material is the high sensitivity of p-SiOCH film during line etching with fluorocarbon based plasma. In this case, fluorine reactive species diffusion and ion bombardment leads to the formation of a hydrophilic layer (bottom and sidewalls), not sealing the pores, and altering the dielectric film properties. While the second problem presented with bottom line roughness formation and explained by intrinsic roughness or micromasking (coming from reactor wall conditioning or FC species and increased by the low volatile compounds (TiFx) coming from the sputtered hard mask) strongly impacts reliability performances like TDDB.

The common solution to limit these issues is to develop high polymerising chemistry at high substrate temperature above 50°C. Developing etching processes at substrate temperature above 50°C allows limiting sputtered metal species condensation leading to micromasking. While the use of high polymerising chemistry leads to the formation of thick fluorocarbon layers which act as protective layers against fluorine diffusion inside the porous SiOCH material and ion bombardment impact but also protect the metallic hard mask and smooth the p-SiOCH film. In addition a complementary solution to limit the impact of the film modification is the restoration of the hydrophobic properties of the modified layer using silylation process.

References

1. M. R. Baklanov and K. Maex, 206. Phil. Trans. R. Soc. A (2006)
2. D. Shamiryan, T. Abell, F. Iacopi and K. Maex, Mat. Today, N1, 34 (2004)
3. D. Fuard, O. Joubert, L. Vallier and M. Bonvalot, J. Vac. Sci. Technol. B, **19,** 447, (2001)
4. M. Fayolle, G. Passemard, O. Louveau, F. Fusalba, J. Cluzel, journal Microelectronic Eng., **70**, 255, (2003).
5. Willi Volksen, Robert D. Miller and G. Dubois, Chemical Reviews, 110, 56, (2010).
6. A. Grill, D. Edelstein, D. Restaino, M. Lane, S. Gates, E. Liniger, T. Shaw, X.-H. Liu, D. Klaus, V. Patel, S. Cohen, E. Simonyi, N. Klymko1, S. Lane, K. Ida, S. Vogt, T. Van Kleeck, C. Davis, M. Ono, T. Nogami, T. Ivers, in: International Interconnect Technology Conference , 54 (2004).
7. N. Posseme, T. Chevolleau, O. Joubert, L. Vallier, N. Rochat. J. Vac. Sci. Technol. B, **22**, 2772, (2004).
8. D. L. Keil, B. A. Hemer and S. Lassig, J. Vac. Sci. Technol. B, **21,** 1969 (2003).

9. N. Posseme, C. Maurice, Ph. Brun, E. Ollier, M. Guillermet, C. Verove, T. Berger, R. Fox, and O. Hinsinger, International interconnect technology conference (IITC) proceedings, 36 (2006).
10. H. Struyf, D. Hendrickx, J. Van Olmen, F. Iacopi, O. Richard, Y. Travaly, M. Van Hove, W. Boullart and S. Vanhaelemeersch, International interconnect technology conference (IITC) proceedings, 30 (2005).
11. M. Darnon, T. Chevolleau, D. Eon, R. Bouyssou, B. Pelissier, L. Vallier, O. Joubert, N. Posseme, T. David, F. Bailly, J. Torres, Microelectronic Eng. **85**, 2226, (2008).
12. A. Zenasni, B. Remiat, C. Waldfried, C. Le Cornec, V. Jousseaume, and G. Passemard, Thin Solid Films, **516**, 1097, (2008).
13. V. Jousseaume, L. Favennec, A. Zenasni, and O. Gourhant, Surf. Coat. Technol., **201**, 9248 (2007).
14. N. Posseme, T. Chevolleau, O. Joubert, L. Vallier, P. Mangiagalli., J. Vac. Sci. Technol. B, **21**, 2432, (2003).
15. Pargon, E. and O. Joubert, J. Vac. Sci. Technol. B, **22**, 1869, (2004).
16. N.Rochat, M.Olivier, A.Chabli, F.Conne, G.Lefeuvre, C.Boll-Burdet, Applied Physics Lett. **77**, 2249, (2000).
17. N. Rochat, A. Troussier, A. Hoang and F. VinetMaterials Science and engineering, **23**, 99, (2003).
18. Q. T. Le, M. R. Baklanov, E. Kesters, A. Azioune, H. Struyf, W. Boullart, J. -J. Pireaux, S. Vanhaelemeersch., Electrochem. Solid-State Lett. **8**, F21, (2005).
19. O. Louveau, C. Bourlot, A. Marfoure, I. Kalinovski, J. Su, G. H. Hills and D. Louis, Microelectronic Eng., **73**,351, (2004).
20. N. Posseme, T. Chevolleau, T. David, M. Darnon, O. Louveau and O. Joubert, J. Vac. Sci. Technol. B. **25** , 1928, (2007).
21. C. Licitra, F. Bertin, M. Darnon, T. Chevolleau, C. Guedj, S. Cetre, H. Fontaine, A. Zenasni, L. L. Chapelon, Physica Status Solidi, **5**, 1278, (2008).
22. W. Puyrenier, V. Rouessac, L. Broussous, D. Rébiscoul, A. Ayral, Microporous Mesoporous Mat. 106, 40, (2007).
23. R. Bouyssou, M. El Kodadi, C. Licitra, T. Chevolleau, M. Besacier, N. Posseme, O. Joubert, P. Schiavone, J. Vac. Sci. Technol. B. **28**,31, (2010)
24. A. Bourgeois, Y. Turcant, C. Walsh, and C. Defranoux, Adsorption-Journal of the International Adsorption Society **14**, 457, (2008).
25. F.Bailly, T. David, T. Chevolleau, M. Darnon, N. Posseme, R. Bouyssou, J. Ducote, O. Joubert, and C. Cardinaud, J. Appl. Phys. **108**, 014906 (2010).
26. Theil, J. A. Tsu, D. V. Watkins, M. W. Kim, S. S. Lucovsky, G. J. Vac. Sci. Technol. A **8,** 1374 (1990).
27. A. Goullet, C. Vallee, A. Granier, G. Turban, J. Vac. Sci. Technol. A **18,** 2452 (2000).
28. H. Chaabouni, L.L. Chapelon, M. Aimadeddine, J. Vitiello, A. Farcy, R. Delsol, P. Brun, D. Fossati, V. Arnal, T. Chevolleau, O. Joubert, J. Torres, Microelectronic Eng. **84**, 2595, (2007).
29. M. Darnon, T. Chevolleau, T. David, J. Ducote, N. Posseme, R. Bouyssou, F. Bailly, D. Perret, and O. Joubert. J. Vac. Sci. Technol. B **28**, 149 (2010).
30. P. Lazzeri, X. Hua, G. S. Oehrlein, M. Barozzi, E. Iacob, and M. Anderle, J. Vac. Sci. Technol. B **23**, 1491 (2005).
31. Y. Yin and H. H. Sawin, J. Vac. Sci. Technol. A **25**, 802 (2007).
32. Y. Yin and H. H. Sawin, J. Vac. Sci. Technol. A **26**, 151 (2008).

33. G. M. Gallatin and C. B. Zarowin, J. Appl. Phys. **65**, 5078, (1989).
34. W. W. Mullins, J. Appl. Phys. **30**, 77 (1959).
35. R. P. U. Karunasiri, R. Bruinsma, and J. Rudnick, Phys. Rev. Lett. **62**, 788 (1989).
36. J. H. Yao and H. Guo, Phys. Rev. E 47, 1007 (1993).
37. C. Roland and H. Guo, Phys. Rev. Lett. **66**, 2104 (1991).
38. G. S. Bales and A. Zangwill, Phys. Rev. Lett. **63**, 692 (1989).
39. M. Martin and G. Cunge, J. Vac. Sci. Technol. B **26**, 1281 (2008).
40. J. T. Drotar, Y.-P. Zhao, T.-M. Lu, and G.-C. Wang, Phys. Rev. B **61**, 3012 (2000).
41. E. Zakka, V. Constantoudis, and E. Gogolides, IEEE Trans. Plasma Sci. 35, 1359 (2007).
42. M. Schaepkens, G. S. Oehrlein, C. Hedlund, L. B. Jonsson, and H.-O. Blom, J. Vac. Sci. Technol. A **16**, 3281 (1998).
43. D. Flamm and D. Manos, Plasma Etching: An Introduction (Academic, New York, 1989).
44. Y.-P. Zhao, J. T. Drotar, G.-C. Wang, and T.-M. Lu, Phys. Rev. Lett. **82**, 4882 (1999).
45. G. S. Hwang, C. M. Anderson, M. J. Gordon, T. A. Moore, T. K. Minton, and K. P. Giapis, Phys. Rev. Lett. **77**, 3049 (1996).
46. R. Pétri, P. Brault, O. Vatel, D. Henry, E. André, P. Dumas, and F. Salvan, J. Appl. Phys. **75**, 7498 (1994).
47. E. Gogolides, C. Boukouras, G. Kokkoris, O. Brani, A. Tserepi, and V.Constantoudis, Microelectron. Eng. 73–74, 312 (2004).
48. Y. Yin, S. Rasgon, and H. H. Sawin, J. Vac. Sci. Technol. A, **24**, 2360 (2006).
49. T. Tatsumi and K. Urata, J. Vac. Sci. Technol. A **23**, 938 (2005).
50. N. Posseme, T. David, M. Darnon, T. Chevolleau, and O. Joubert, 6th International Conference on Microelectronics and Interfaces, 2005
51. M. Darnon, T. Chevolleau, D. Eon, R. Bouyssou, B. Pelissier, L. Vallier, O. Joubert, N. Posseme, T. David, F. Bailly, and J. Torres, Microelectron. Eng. **85**, 2226 (2008).